Tsunami simulation technique considering dynamic seabed displacement and acoustic effects of water

Tatsuo Ohmachi[1], Shusaku Inoue[1], Hiroyuki Matsumoto[1], and Hiroshi Tsukiyama[2]

[1]***Department of Built Environment, Tokyo Institute of Technology, Midori-ku, Yokohama, Japan***

[2]***Tsukiyama Research, Inc., Funabashi, Chiba, Japan***

Abstract. In conventional tsunami simulation technique, dynamic seabed displacement resulting from seismic fault rupturing has been neglected and only static contribution has been considered. The seawater is assumed to be incompressible regardless of its acoustic effects. These simplifications should be reconsidered in light of state-of-the-art technology when there is considerable difference between numerical simulation and actual observation. In the present study, tsunami simulation is conducted without using these simplifications. Both dynamic and static displacements of the ground surface caused by the oceanic seismic faulting are simulated first by the boundary element method. Then, by applying velocity associated with the displacements at the bottom of the seawater, water waves are simulated by the finite difference method taking into account acoustic effects. As a result, the simulated tsunami is found to be remarkably larger in the wave height, especially in the near-fault area where effects of the dynamic displacement and acoustic waves are superposed. In the far-fault area, however, there is little difference from tsunami height given by the conventional technique. Finally, the present tsunami simulation technique is applied to an actual tsunami caused by the 1983 Nihonkai-Chubu earthquake.

1. Introduction

There are important problems still unsolved in the boundary areas of earthquake engineering and coastal engineering. For example, there has been large discrepancy between fault models of an earthquake estimated from seismic data and those from tsunami data. The discrepancy may be attributed to conventional approximation used in tsunami simulation. According to conventional tsunami simulation technique, an initial sea surface profile is assumed to be the same as the static (residual) displacement caused by seismic faulting, and wave propagation is approximated with long waves.

In recent years, the authors have developed a new technique to simulate tsunami generation followed by propagation, without using the conventional approximation. To check the validity and draw some findings, our technique is applied to simulation of a tsunami caused by two different types of source mechanism and an actual tsunami due to the 1983 Nihonkai-Chubu, Japan earthquake.

[1]Tokyo Institute of Technology, Department of Built Environment, 4259, Nagatsuta-cho, Midori-ku, Yokohama 226-8502, Japan (ohmachi@enveng.titech.ac.jp, shusaku@nf.enveng.titech.ac.jp, matsumo@enveng.titech.ac.jp)

[2]Tsukiyama Research, Inc., 4-18-2, Narashino-dai, Funabashi, Chiba, 274-0063-303, Japan (pxi10213@niftyserve.or.jp)

2. Outline of Formulation of the Technique

In the present technique, a total system consisting of the seawater and the underlying ground is assumed to be a weakly coupled system. On this assumption, earthquake ground motion due to seismic fault rupturing is first simulated by the boundary element method (BEM) (Kataoka, 1996). Then, seawater disturbance, including tsunamis resulting from the seismic ground motion, is simulated by the finite difference method (FDM) using the ground motion velocity as an input to the seawater. Formulation of these methods are outlined here with a main focus on application to the present technique.

2.1 Ground motion analysis

Differential equations for elastic waves in the frequency domain are written as

$$(\lambda+\mu)u_{j,ij}+\mu\,u_{i,jj}+\rho\,\omega^2 u_i+\bar{b}_i=0 \tag{1}$$

where u_i is displacement, λ and μ are Lame's constants, ρ is mass density, ω is circular frequency, and $\bar{b}_i$ is body force. A weighted-residual expression of (1) is given by

$$\begin{aligned}\int_\Omega \big\{&(\lambda+\mu)u_{k,jk}(\boldsymbol{x}_0)+\mu\,u_{j,kk}(\boldsymbol{x}_0)+\rho\,\omega^2 u_j(\boldsymbol{x}_0)\\ &+\bar{b}_j(\boldsymbol{x}_0)\big\}\,U_{ij}(\boldsymbol{x},\boldsymbol{x}_0)\,d\Omega(\boldsymbol{x}_0)=0\end{aligned} \tag{2}$$

When the Gauss theorem is used, Eq. (2) is rewritten as

$$\begin{aligned}\int_\Omega &\{(\lambda+\mu)U_{ik,jk}(\boldsymbol{x},\boldsymbol{x}_0)+\mu U_{ij,kk}(\boldsymbol{x},\boldsymbol{x}_0)\\ &+\rho\,\omega^2 U_{ij}(\boldsymbol{x},\boldsymbol{x}_0)\big\}\,u_j(\boldsymbol{x}_0)\,d\Omega(\boldsymbol{x}_0)\\ &-\int_\Gamma T_{ij}(\boldsymbol{x},\boldsymbol{x}_0)u_j(\boldsymbol{x}_0)\,d\Gamma(\boldsymbol{x}_0)+\int_\Gamma U_{ij}(\boldsymbol{x},\boldsymbol{x}_0)\tau_j(\boldsymbol{x}_0)\,d\Gamma(\boldsymbol{x}_0)\\ &+\int_\Omega U_{ij}(\boldsymbol{x},\boldsymbol{x}_0)\bar{b}_j(\boldsymbol{x}_0)\,d\Omega(\boldsymbol{x}_0)=0\end{aligned} \tag{3}$$

where τ_i and T_{ij} are traction and its Green function expressed as

$$\tau_i = \{\lambda u_{m,m}\delta_{jk}+\mu(u_{i,k}+u_{k,i})\}n_k \tag{4}$$

$$T_{ij} = \{\lambda U_{im,m}\delta_{jk}+\mu(U_{ij,k}+U_{ik,j})\}\,n_k \tag{5}$$

A Green function for (1) satisfies (6)

$$\begin{aligned}&(\lambda+\mu)U_{ik,jk}(\boldsymbol{x},\boldsymbol{x}_0)+\mu U_{ij,kk}(\boldsymbol{x},\boldsymbol{x}_0)+\rho\,\omega^2 U_{ij}(\boldsymbol{x},\boldsymbol{x}_0)\\ &\quad=-\delta_{ij}\delta_D(\boldsymbol{x}-\boldsymbol{x}_0)\end{aligned} \tag{6}$$

where δ_D is the dirac delta function. Substituting (6) into (3) leads to

$$\begin{aligned}-&\int_\Gamma T_{ij}(\boldsymbol{x},\boldsymbol{x}_0)u_j(\boldsymbol{x}_0)\,d\Gamma(\boldsymbol{x}_0)+\int_\Gamma U_{ij}(\boldsymbol{x},\boldsymbol{x}_0)\tau_j(\boldsymbol{x}_0)\,d\Gamma(\boldsymbol{x}_0)\\ +&\int_\Omega U_{ij}(\boldsymbol{x},\boldsymbol{x}_0)\bar{b}_j(\boldsymbol{x}_0)\,d\Omega(\boldsymbol{x}_0)\\ =&\begin{cases}u_i(\boldsymbol{x}) & (\boldsymbol{x}\in\Omega)\\ 0 & (\boldsymbol{x}\notin\Omega)\end{cases}\end{aligned} \tag{7}$$

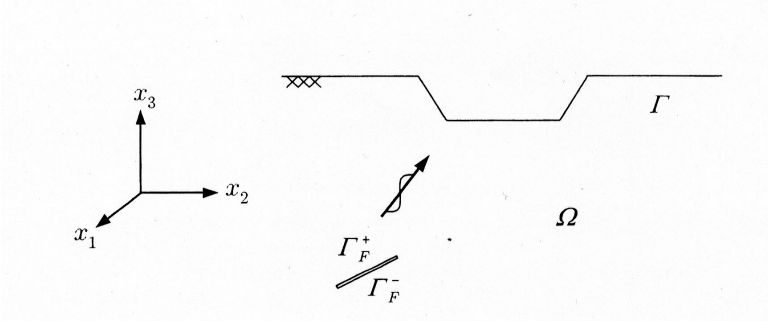

Figure 1: Seismic faulting and irregular ground.

This is called the Somigliana equation. When seismic waves are radiated from a seismic fault, and is incident to the irregularly shaped ground as shown in Fig. 1, the following boundary equation holds along the Γ,

$$\begin{aligned} c_{ij}(\boldsymbol{x})\, u_j(\boldsymbol{x}) + \int_\Gamma T_{ij}(\boldsymbol{x}, \boldsymbol{x}_0)\, u_j(\boldsymbol{x}_0)\, d\Gamma(\boldsymbol{x}_0) \\ - \int_\Gamma U_{ij}(\boldsymbol{x}, \boldsymbol{x}_0)\, \tau_j(\boldsymbol{x}_0)\, d\Gamma(\boldsymbol{x}_0) \\ = \bar{\psi}_i(\boldsymbol{x}) \end{aligned} \tag{8}$$

where c_{ij} is a constant determined from the shape of the boundary. When dislocation of the fault is considered, the dislocation vector along the fault is given by

$$d_i(\boldsymbol{x}_F) = u_i^+(\boldsymbol{x}_F) - u_i^-(\boldsymbol{x}_F) \tag{9}$$

where $\boldsymbol{x}_F$ is a point on the fault. Then, the term $\bar{\psi}_i$ in (8) is determined from

$$\bar{\psi}_i(\boldsymbol{x}) = \int_{\Gamma_F} T_{ij}(\boldsymbol{x}, \boldsymbol{x}_F)\, d_j(\boldsymbol{x}_F)\, d\Gamma(\boldsymbol{x}_F) \tag{10}$$

2.2 Water wave analysis

The Navier-Stokes equation for viscous fluid is given by

$$\frac{\partial \boldsymbol{u}}{\partial t} + (\boldsymbol{u} \cdot \nabla)\ \boldsymbol{u} = -\frac{1}{\rho} \nabla p + \nu \nabla^2 \boldsymbol{u} \tag{11}$$

where ν is viscosity. A mass conservation equation for compressive fluid is given by

$$\frac{\partial \rho}{\partial t} + \rho\, (\nabla \cdot \boldsymbol{u}) = 0 \tag{12}$$

When limited compressibility is assumed for the fluid, a state equation expressed as

$$\rho = f\,(p, E) \tag{13}$$

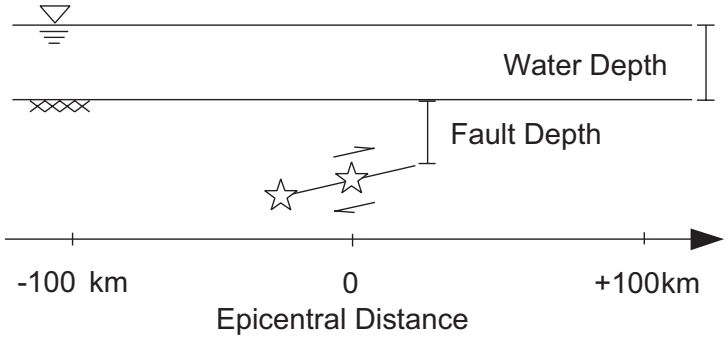

Figure 2: Two-dimensional tsunami simulation model.

can be employed. Acoustic wave velocity of the water is given by

$$a = \sqrt{\frac{\partial p}{\partial \rho}} \tag{14}$$

Using (13) and (14), (12) can be rewritten as

$$\frac{1}{a^2}\frac{\partial p}{\partial t} + \rho\left(\frac{\partial u}{\partial x} + \frac{\partial v}{\partial y} + \frac{\partial w}{\partial z}\right) = 0 \tag{15}$$

Equations (11) and (15) are solved by applying the leap-frog scheme.

3. Two-Dimensional Simulation of Two Different Types of Source Mechanism

Effects of source mechanism on tsunamis are evaluated in 2 dimensions. Two types of rupture propagation are considered for thrust faulting in an elastic half-space. One is unilateral faulting, in which the fault rupture starts at the bottom of a fault and propagates upward. The other is bilateral faulting, in which the fault rupture starts at the middle of the fault and propagates both upward and downward. Figure 2 and Table 1 shows the analytical model and parameters of the seismic fault and the ground. Simulation area extends to ±100 km from the epicenter. Water depth is kept constant at 3000 m.

The frequency range for the simulation of the ground motion is between DC and 4 Hz. Until 128 s after the fault rupturing, velocity of the ground motion is input at the bottom of the fluid domain.

In the simulation of the fluid domain, the grid sizes and time step are set to 1 km and 0.4 km in horizontal and vertical directions, and 0.25 s, respectively.

3.1 Unilateral faulting

Figure 3 shows the snapshots at several seconds after the fault rupturing in the case of the unilateral faulting. The lower and upper surfaces represent the

Table 1: Parameters of the fault and the ground.

Width	30 km
Fault depth	7 km
Dip	30°
Dislocation	10 m
Rupture velocity	3.0 km/s
Rise time	2.0 s
P-wave velocity	7.0 km/s
S-wave velocity	4.0 km/s

seabed and the sea surface, respectively. At 14 s after the fault rupturing, the maximum uplift of 789 cm occurs in the near-fault area, which is 1.7 times as large as the static displacement. From 20 s to 30 s, the Rayleigh wave is generated in the near-fault area and is propagated along the seabed to the right of the figure (footwall side), giving rise to short-period water waves that can travel with the same speed as the Rayleigh wave. At 50 s, the profile of the tsunami remaining in the near-fault area is similar to that from the static seabed displacement.

Thus the dynamic seabed displacement and the acoustic wave are found to give a remarkable increase in the water wave height, especially in the near-fault area, as a result of superposed effects of the dynamic and static seabed displacements. According to the present simulation, the short-period water wave is induced by the Rayleigh wave and travels mainly on the footwall side of the seabed.

3.2 Bilateral faulting

Figure 4 shows snapshots in the case of bilateral faulting. From the snapshot at 7 s after the fault rupturing, the uplift is seen earlier than that in Fig. 3 because of the shallower hypocenter. A considerable difference can be seen between water waves from the unilateral faulting and those from the bilateral faulting. After 15 s, the Rayleigh wave appears and propagates in both the footwall and hanging wall sides. Likewise, sea waves induced by the Rayleigh wave also propagate in both sides. In the meantime, the tsunami in the far-fault area is almost the same in both cases.

4. Simulation of an Actual Tsunami Due to the 1983 Nihonkai-Chubu Earthquake

Next, the present technique is applied to an actual tsunami caused by the 1983 Nihonkai-Chubu, Japan, earthquake. The Nihonkai-Chubu earthquake (M 7.7) occurred at 11:59 JST (Japan Standard Time) on 26 May 1983.

A fault model proposed by Aida (1984) which was based on tidal records and tsunami run-ups is quite different from a seismically determined model proposed by Sato (1985). In the present simulation, the latter model is used.

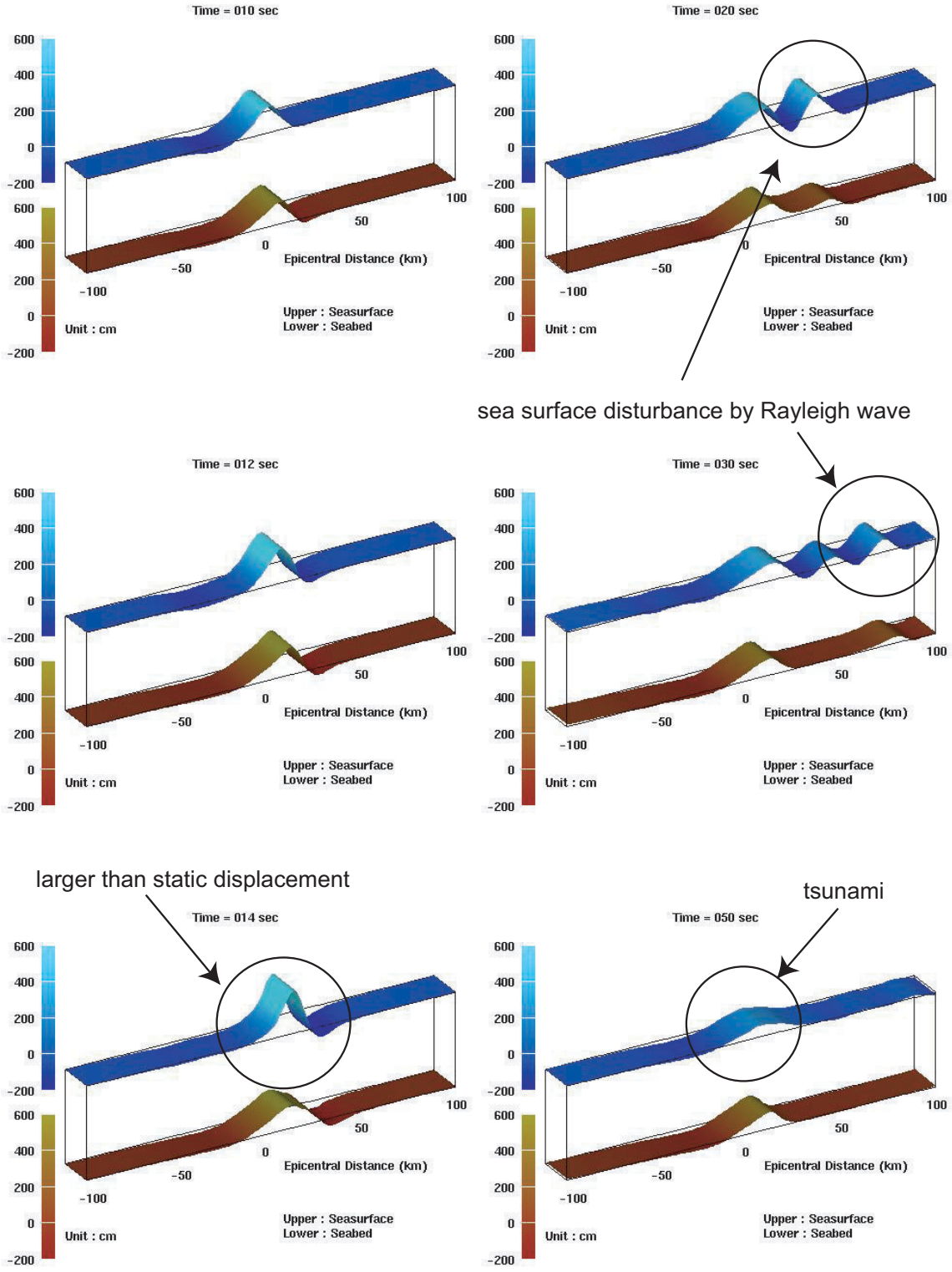

Figure 3: Two-dimensional tsunami simulation in the case of unilateral faulting. The lower and upper surfaces represent the seabed and the sea surface.

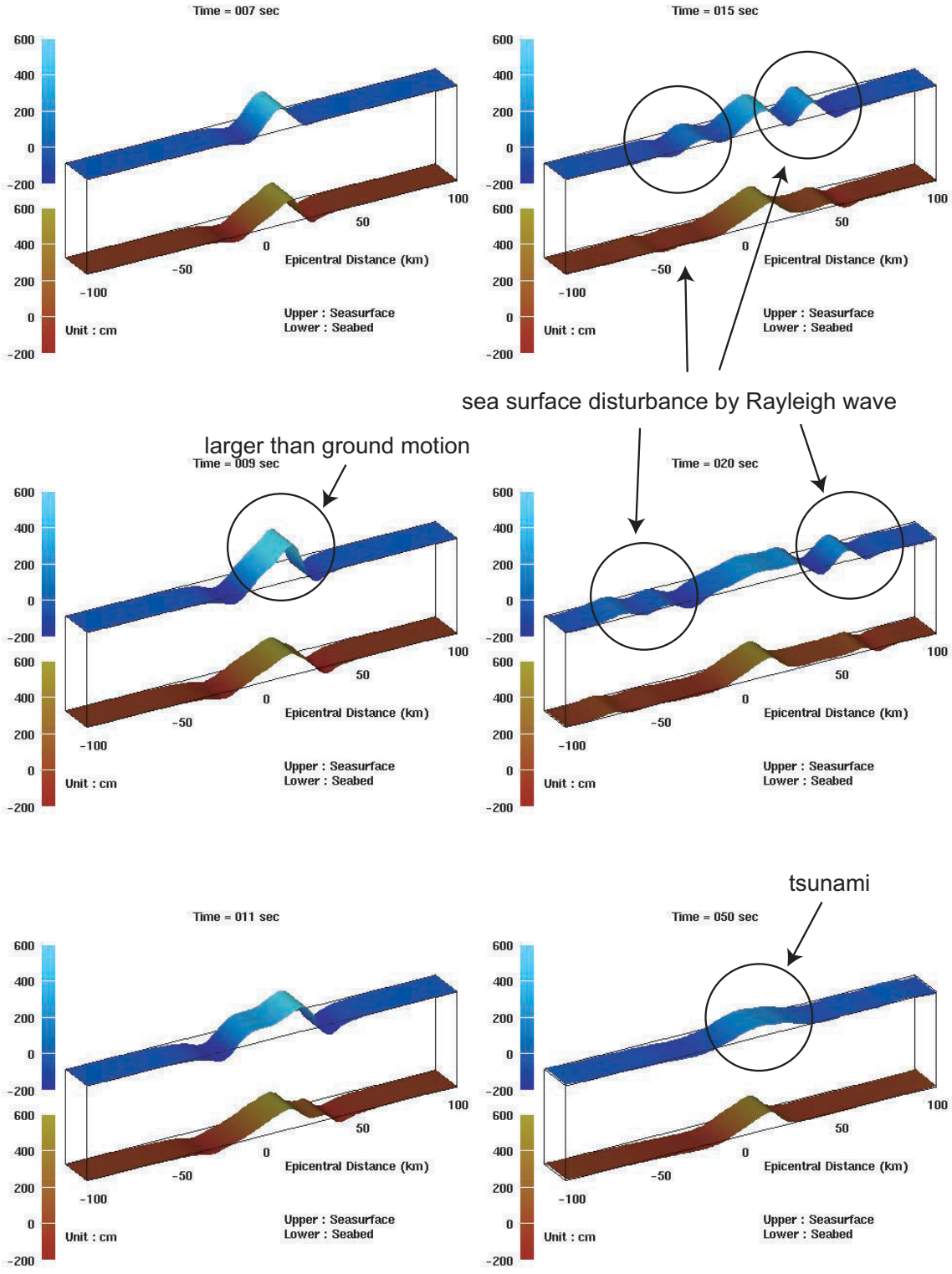

Figure 4: Two-dimensional tsunami simulation in the case of bilateral faulting. The lower and upper surfaces represent the seabed and the sea surface.

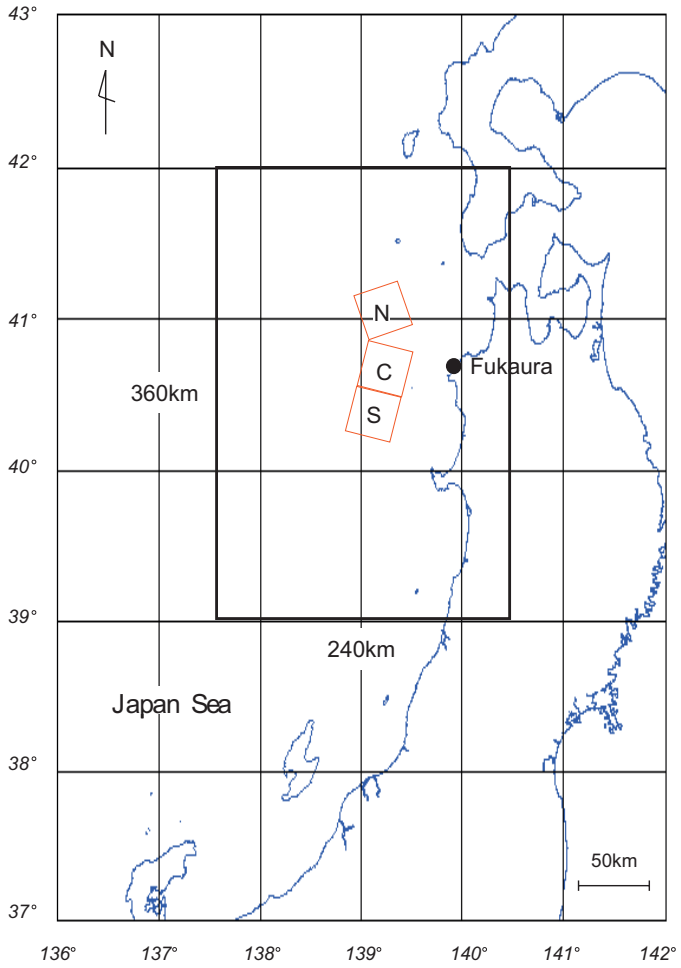

Figure 5: Fault planes projection assumed about the 1983 Nihonkai-Chubu, Japan earthquake, and calculation area.

Table 2: Fault parameters.

	Southern	Central	Northern
Seismic moment (dyne/cm)	3×10^{27}	2×10^{27}	3×10^{27}
Fault length (km)	35	35	35
Fault width (km)	35	35	35
Top depth (km)	0	0	0
Strike (degree)	15	15	345
Dip (degree)	20	20	20
Rake (degree)	90	90	90
Dislocation (m)	6.8	4.6	6.8
Rupture velocity (km/s)	2.0	2.0	3.0
Rise time (s)	3.5	3.5	3.0

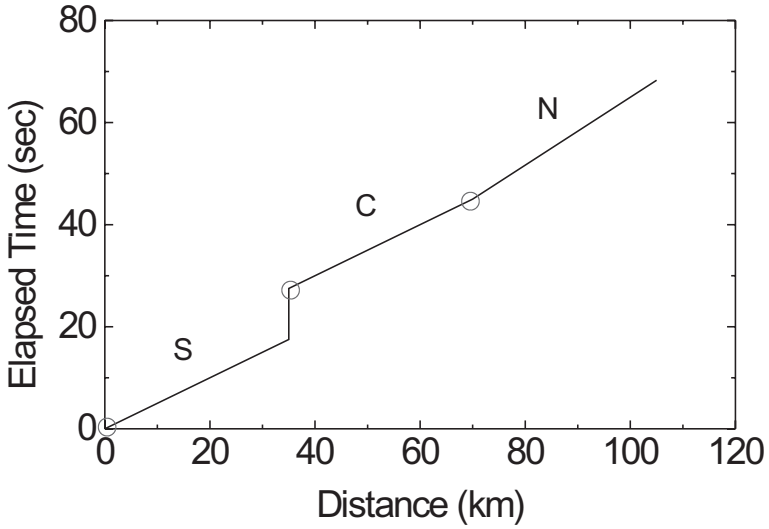

Figure 6: Relation between elapsed time and rupture distance.

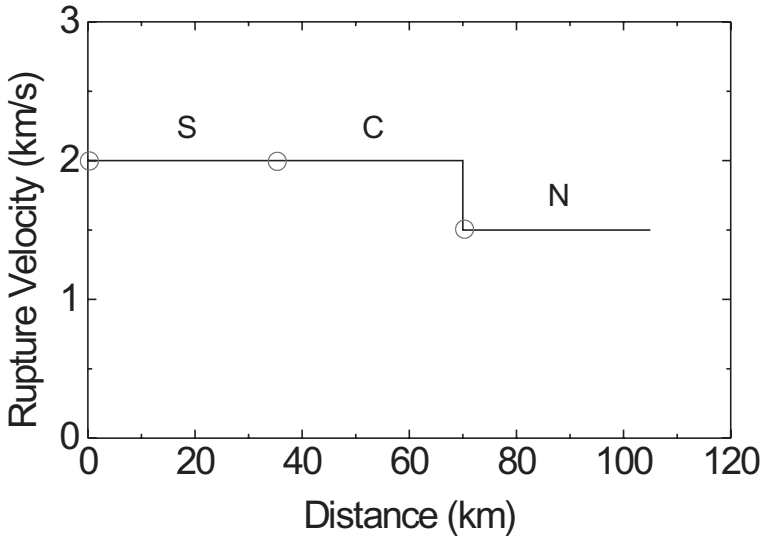

Figure 7: Relation between rupture velocity and rupture distance.

The fault projection, the calculation area, and the fault parameters are shown in Fig. 5 and Table 2. The simulation area is 360 km long in the NS direction and 240 km wide in the EW direction. The grid size for the seabed and water layer is 5 km and 1 km, respectively. The three-step fault rupturing (event) is assumed as shown in Fig. 6 and Fig. 7. The first rupturing starts at the southern edge and develops in the NNE direction with a velocity of 2 km/s. After a pause of about 10 s, the second fault rupturing starts to extend in the same direction and consequently the third fault rupturing starts to develop in the NNW direction with a velocity of 1.5 km/s. The total duration time of the fault rupturing is 63 s.

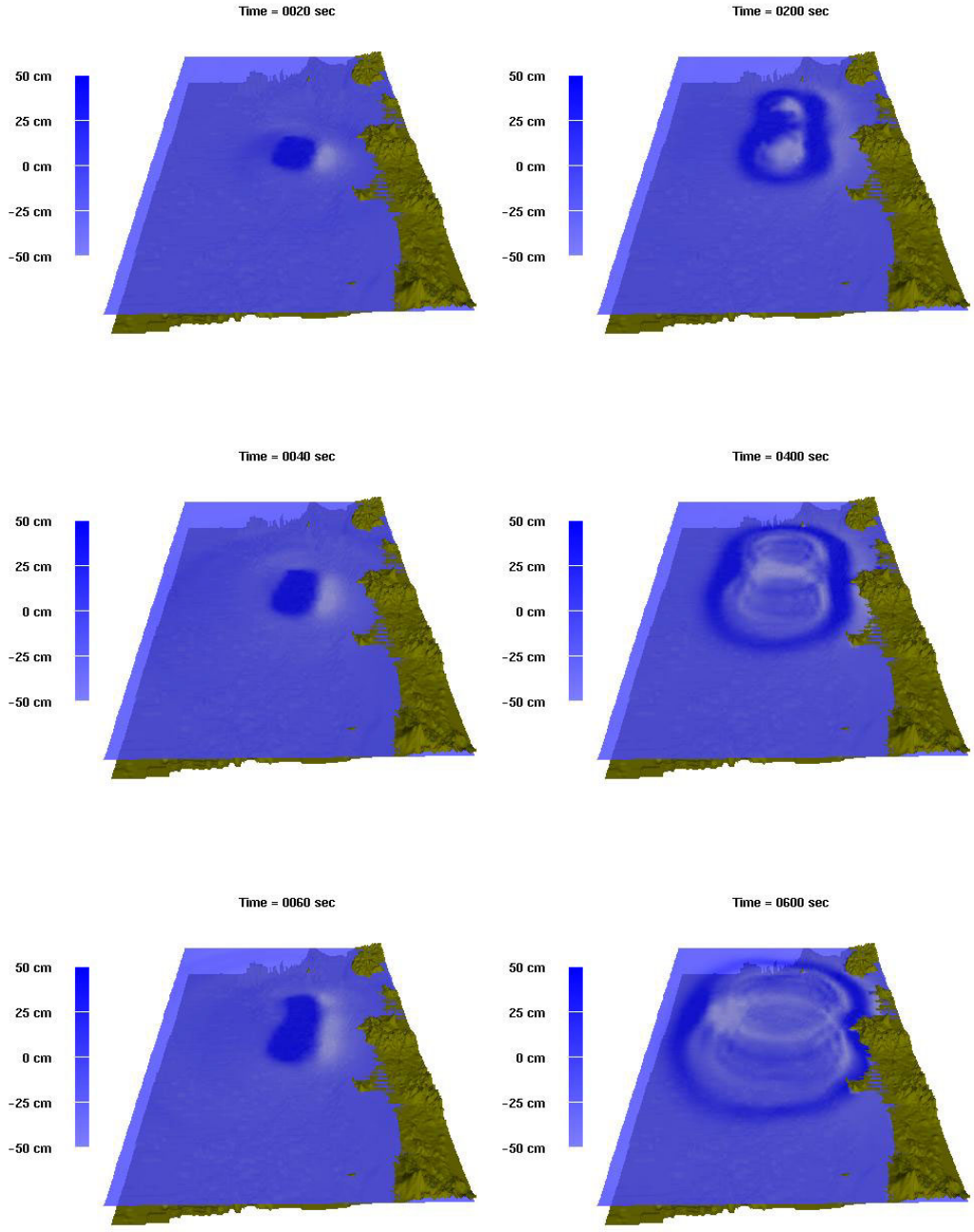

Figure 8: Three-dimensional tsunami simulation about the 1983 Nihonkai-Chubu, Japan earthquake.

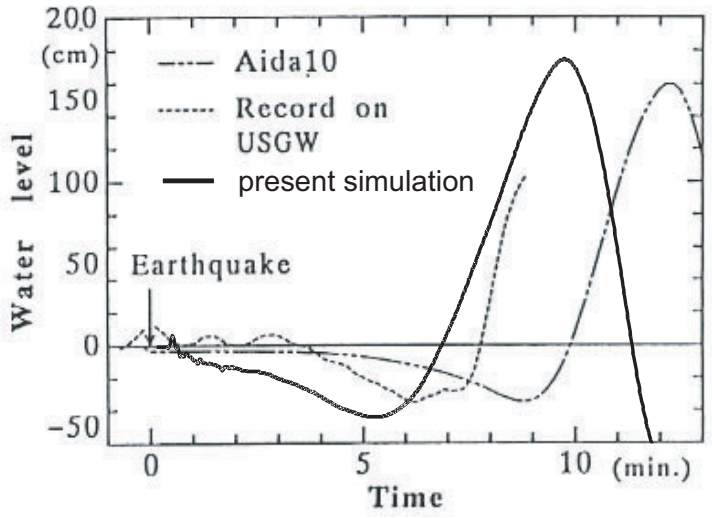

Figure 9: Comparison of the tsunamis observed at Fukaura, simulated by the conventional technique (Shuto *et al.*, 1995) and simulated by the present technique.

Snapshots in Fig. 8 show the simulation results at 20, 40, 60, 200, 400, and 600 s after the fault rupturing. At 20 s the first event generates a tsunami in the southern area. From 20 s to 40 s, the water wave induced by the Rayleigh wave propagates to the north. At 60 s when the fault rupture finishes, static uplift and subsidence remain in the near-fault area, and the tsunami profile is almost the same as that of the static displacement of the seabed.

Thus, the dynamic analysis can demonstrate not only the process of tsunami generation but also the water wave induced by the Rayleigh wave. Actually, before arrival of the first tsunami, the sea surface disturbance was observed in several tidal records along the coast of northern Japan.

During the earthquake several tidal records were obtained, but their resolution with respect to time was very poor (Satake *et al.*, 1988). At Fukaura, whose location is shown in Fig. 5, an ultrasonic wave sensor has also been installed which directly measures the vertical distance between the seabed and the sea surface. The arrival time and profile of the first tsunami can be discussed because it recorded the main portion of the first rise of the tsunami. Fig. 9 compares the tsunamis observed at Fukaura, simulated by the present technique and simulated by the conventional one using Aida's fault model (Shuto *et al.*, 1995). The present simulation is found to be in fairly good agreement with the observation in wave height and arrival time of the first tsunami, as a whole.

5. Conclusion

The following conclusions can be drawn from the present simulation.

1. In the near-fault area, the dynamic ground displacement has the effect

of producing water waves much higher than those estimated from conventional tsunami theory. This is mainly because the dynamic ground displacement can sometimes be two or three times larger both in amplitude and in the extent of the wave source area than the static displacement.

2. Vertical ground displacement associated with Rayleigh waves induces another type of sea wave having a velocity higher than tsunamis. It has special characteristics such as directivity and large velocity, and amplitude which depends on fault parameters and water depth.

3. Tsunami simulation of the 1983 Nihonkai-Chubu earthquake has been performed by using a seismically determined fault model, implying the validity and usefulness of the present technique.

Acknowledgments. The authors wish to thank Professor Imamura, Tohoku University, and Dr. Iwasaki, National Research Institute for Earth Science and Disaster Prevention, Science, and Technology Agency, for their useful discussion. This study was supported by the Ministry of Education, Science, Sports, and Culture, Grant-in-Aid for Scientific Research.

6. References

Aida, I. (1984): A source model of the tsunami accompanying the 1983 Nihonkai-Chubu earthquake. *Bull. Earthq. Res. Inst., 59*, 105–113. (in Japanese)

Kataoka, S. (1996): Development of simulation methods for earthquake motion based on three-dimensional fault-ground models. Ph.D. thesis, Tokyo Institute of Technology.

Satake, K., M. Okada, and K. Abe (1988): Tide gauge response to tsunamis: Measurements at 40 tide gauge stations in Japan. *J. Mar. Res., 46*, 557–571.

Sato, T. (1985): Rupture characteristics of the 1983 Nihonkai-Chubu (Japan Sea) earthquake as inferred from strong motion accelerograms. *J. Phys. Earth, 33*, 525–557.

Shuto, N., K. Chida, and F. Imamura (1995): Generation mechanism of the first wave of the 1983 Nihonkai-Chubu earthquake. In *Tsunami: Progress in Prediction, Disaster Prevention, and Warning*, edited by Y. Tsuchiya and N. Shuto, Kluwer Academic Publishers, 37–53.